Stress Signal Regulation by Na/K-ATPase As a New Approach to Promote Physiological Revascularization in a Mouse Model of Ischemic Retinopathy

Jiayan Wang,[1,2] Xiaoliang Wang,[1,2] Yingnyu Gao,[1] Zhucheng Lin,[1] Jing Chen,[3] James Gigantelli,[2] Joseph I. Shapiro,[2] Zijian Xie,[1,*] and Sandrine V. Pierre[1]

[1]Marshall Institute for Interdisciplinary Research, Marshall University, Huntington, West Virginia, United States
[2]Departments of Medicine, Ophthalmology, Pharmacology, and Surgery, Joan C. Edwards School of Medicine, Marshall University, Huntington, West Virginia, United States
[3]Department of Ophthalmology, Boston Children's Hospital, Harvard Medical School, Boston, Massachusetts, United States

Correspondence: Sandrine V. Pierre, Arthur Weisberg Family Applied Engineering Complex, Marshall University, 1676 3rd Avenue, Huntington, WV 25703, USA; pierres@marshall.edu.

* Deceased January 17, 2020.

Received: June 30, 2020
Accepted: October 30, 2020
Published: December 4, 2020

Citation: Wang J, Wang X, Gao Y, et al. Stress signal regulation by Na/K-ATPase as a new approach to promote physiological revascularization in a mouse model of ischemic retinopathy. *Invest Ophthalmol Vis Sci.* 2020;61(14):9. https://doi.org/10.1167/iovs.61.14.9

Purpose. The identification of target pathways to block excessive angiogenesis while simultaneously restoring physiological vasculature is an unmet goal in the therapeutic management of ischemic retinopathies. pNaKtide, a cell-permeable peptide that we have designed by mapping the site of α1 Na/K-ATPase (NKA)/Src binding, blocks the formation of α1 NKA/Src/reactive oxygen species (ROS) amplification loops and restores physiological ROS signaling in a number of oxidative disease models. The aim of this study was to evaluate the importance of the NKA/Src/ROS amplification loop and the effect of pNaKtide in experimental ischemic retinopathy.

Methods. Human retinal microvascular endothelial cells (HRMECs) and retinal pigment epithelium (ARPE-19) cells were used to evaluate the effect of pNaKtide on viability, proliferation, and angiogenesis. Retinal toxicity and distribution were assessed in those cells and in the mouse. Subsequently, the role and molecular mechanism of NKA/Src in ROS stress signaling were evaluated biochemically in the retinas of mice exposed to the well-established protocol of oxygen-induced retinopathy (OIR). Finally, pNaKtide efficacy was assessed in this model.

Results. The results suggest a key role of α1 NKA in the regulation of ROS stress and the Nrf2 pathway in mouse OIR retinas. Inhibition of α1 NKA/Src by pNaKtide reduced pathologic ROS signaling and restored normal expression of hypoxia-inducible factor 1-α/vascular endothelial growth factor (VEGF). Unlike anti-VEGF agents, pNaKtide did promote retinal revascularization while inhibiting neovascularization and inflammation.

Conclusions. Targeting α1 NKA represents a novel strategy to develop therapeutics that not only inhibit neovascularization but also promote physiological revascularization in ischemic eye diseases.

Keywords: Na/K-ATPase signaling, pNaKtide, ischemic retinopathy, reactive oxygen species, angiogenesis, HIF-1α, VEGF

Ischemic retinopathies, including retinopathy of prematurity (ROP), diabetic retinopathy, retinal vein occlusion, and sickle cell retinopathy, are prevalent causes of visual disability.[1,2] Pathologic neovascularization (NV) triggered by retinal ischemia grows into the vitreous cavity, fails to restore the ischemic tissue with adequate vasculature and metabolic supply, and eventually results in vitreous hemorrhage and tractional retinal detachment.[3,4] Neutralization of angiogenetic factors, such as vascular endothelial growth factor (VEGF), has shown therapeutic success.[1,5] However, anti-VEGF therapy has limitations related to suppression of physiological revascularization.[6] Therefore, identification of alternative pathways that could block excessive angiogenesis and restore physiological vasculature simultaneously may improve current therapies for ischemic retinopathies.

Based on the molecular mechanisms of ischemic retinopathy, recent studies have uncovered key pathologic factors such as hypoxia/ischemia, inflammation, and metabolic switch that influence ocular angiogenesis. The importance of molecular signaling pathways such as VEGF, Nrf2, Wnt, Hedgehog, and retinoic acid-related orphan receptor α (RORα) has also been established in the regulation of both physiological revascularization and pathologic neovascularization in ischemic retinopathy.[7–19] Above all, these studies have either directly or indirectly indicated an important role of reactive oxygen species (ROS).[20] For example, ROS stress contributes to delayed physiological retinal vascular development and vascular attenuation in the first phase of ROP. In the second phase of ROP, intravitreal neovascularization is affected by increased generation of ROS. ROS stress also triggers a metabolic switch and the

activation of inflammatory pathways. Mechanistically, ROS stabilize hypoxia-inducible factor (HIF)-1α and increase the transcription of angiogenic factors such as VEGF.[18,21,22] However, there is a knowledge gap in the current understanding of how pathologic ROS signaling is turned on/off in the retina. Moreover, although much has been learned about how to inhibit pathologic neovascularization, little is known about how to promote physiological revascularization in ischemic retinopathies.

Na/K-ATPase (NKA) was discovered by J.C. Skou in 1957.[23] To the best of our knowledge, our group was the first to recognize the enzymatic activity-independent signaling function of Na/K-ATPase and to report that α1 Na/K-ATPase and Src kinase form a functional receptor.[24] We have further documented that the binding of cardiotonic steroids to this receptor complex activates Src, resulting in the transactivation of epidermal growth factor receptor (EGFR) and a number of protein kinase and lipid kinase cascades.[25] It also increases cellular generation of ROS through the activation of both plasma membrane nicotinamide adenine dinucleotide phosphate oxidase and the mitochondrial pathway,[26–28] both of which are involved in ROS generation in response to hypoxia/ischemia in the retina.[12,20,29] We have further demonstrated that the NKA/Src complex itself can serve as a receptor mechanism for ROS to activate Src and further increase ROS generation, which is at least in part due to H_2O_2-induced carbonylation of two specific residues in the A domain of NKA.[30–32] Hence, α1 NKA, Src, and ROS form a positive feed-forward loop, taking part in pathologic ROS signaling regardless of which pathway the signal emanates from.

By mapping the site of α1 NKA/Src interaction, we have discovered the NaKtide sequence as a specific Src binding site. We have subsequently invented the cell-permeable pNaKtide by transactivator of transcription (Tat)-tagging NaKtide and demonstrated that pNaKtide is a potent and effective inhibitor of the α1 NKA/Src.[24,32,33] Pharmacologically, pNaKtide does not affect the enzymatic activity and cellular ion-pumping capacity of NKA or physiological ROS signaling, but it does block the formation of the α1 NKA/Src/ROS amplification loop.[34–37] Consistently, pNaKtide effectively abolishes ROS stress and consequently inhibits inflammation and tissue fibrosis.[33–36] We found that pNaKtide inhibits human endothelial cell proliferation in vitro and also inhibits angiogenesis in a xenograft tumor model.[33]

In view of the well-established role of ROS in the development of ischemic retinopathies and the anti-neovascular effects of pNaKtide in the tumor model, we hypothesized that the α1 NKA/Src complex plays an important role in retinal oxidative stress signaling and is involved in the pathogenesis of ischemic retinopathy. As a corollary, we surmised that blocking the α1 NKA/Src/ROS amplification loop with pNaKtide would attenuate ischemic damage to the retina as evidenced by normalization of both avascular area and neovascularization. Our findings reveal an important role of α1 NKA in the regulation of ROS stress and Nrf2 pathway in the retina. Inhibition of α1 NKA/Src by pNaKtide blocks pathologic ROS signaling, restores normal expression of HIF-1α/VEGF in oxygen-induced retinopathy (OIR) in the mouse, an animal model of ischemic retinopathy. Unlike anti-VEGF agents, not only does pNaKtide promote retinal revascularization, but it also inhibits neovascularization and inflammation.

Methods

Cell Culture and Incubation Protocol

Human retinal microvascular endothelial cells (HRMECs) and human retinal pigment epithelium (ARPE-19) cells were purchased from Cell Systems (CSC 2M1; Kirkland, WA, USA) and American Type Culture Collection (CRL-2302; Manassas, VA, USA), respectively. EGM-2 Medium and HyClone Dulbecco's Modified Eagle Medium/Nutrient Mixture F-12 (DMEM-F12) were purchased from Lonza (CC-3162; Basel, Switzerland) and Cytiva (SH30023.01; Marlborough, MA, USA), respectively. HRMECs were cultured in EGM-2 Medium supplemented with growth factors (CC-4176, Lonza), 5% fetal bovine serum, 100 units/mL penicillin, and 100 µg/mL streptomycin. ARPE-19 cells were cultured in DMEM-F12 media supplemented with 10% fetal bovine serum, 100 units/mL penicillin, and 100 µg/mL streptomycin. Cells were kept at 37°C in humidified air with 5% CO_2. HRMECs and ARPE-19 cells were treated with or without pNaKtide or a scrambled peptide with a Tat leader sequence (Tat-scrambled peptide, sequences listed in Supplementary Table S1), at a concentration of 0.5, 1, or 5 µM for 24 hours. A Trypan blue exclusion assay was performed to evaluate cell viability.

BrdU Assay

Bromodeoxyuridine (BrdU) is a thymidine nucleotide analog that is incorporated (instead of thymidine) during S-phase only in the DNA of proliferating cells. HRMECs were plated in 12- well, collagen-coated chamber slides at a density of 10,000 cells/well. After overnight incubation at 37°C, the medium was changed to EGM-R Medium. The cells were treated with the indicated concentrations of the peptides in EGM-R for 24 hours at 37°C. Cells that were not treated with either one of the peptides served as control/reference. After treatment for 24 hours, the BrdU assay was performed with a BrdU labeling and detection kit (11299964001; Roche Biochemicals, Indianapolis, IN, USA), according to the manufacturer's recommendations. The number of BrdU-positive cells was determined in three independent fields per sample by a blinded investigator. The total number of cells was assessed using 4′,6-diamidino-2-phenylindole (DAPI) counterstaining as we have previously described.[38] Of note, the BrdU kit is based on an immunohistochemical reaction that involves denaturation of DNA with nucleases to increase the sensitivity of BrdU immunological detection. As a result, DAPI counterstaining is generally weaker in BrdU-positive cells, as shown in Figure 1. The fraction of BrdU-positive cells in the control untreated cells was normalized to 1. The relative number of BrdU-positive cells in the peptide-treated HRMECs was calculated as a fraction of the BrdU-incorporated HRMECs. Each sample was tested in triplicate, and the BrdU assay was performed three independent times per group.

Matrigel Studies

BD Matrigel Matrix Growth Factor Reduced (GFR) (BD Biosciences, San Jose, CA, USA) was used to promote the differentiation of HRMECs into capillary tube–like structures. A total of 100 µL of thawed BD Matrigel Matrix GFR was added to 96-well tissue culture plates, followed by incubation at 37°C for 60 minutes to allow

Investigative Ophthalmology & Visual Science

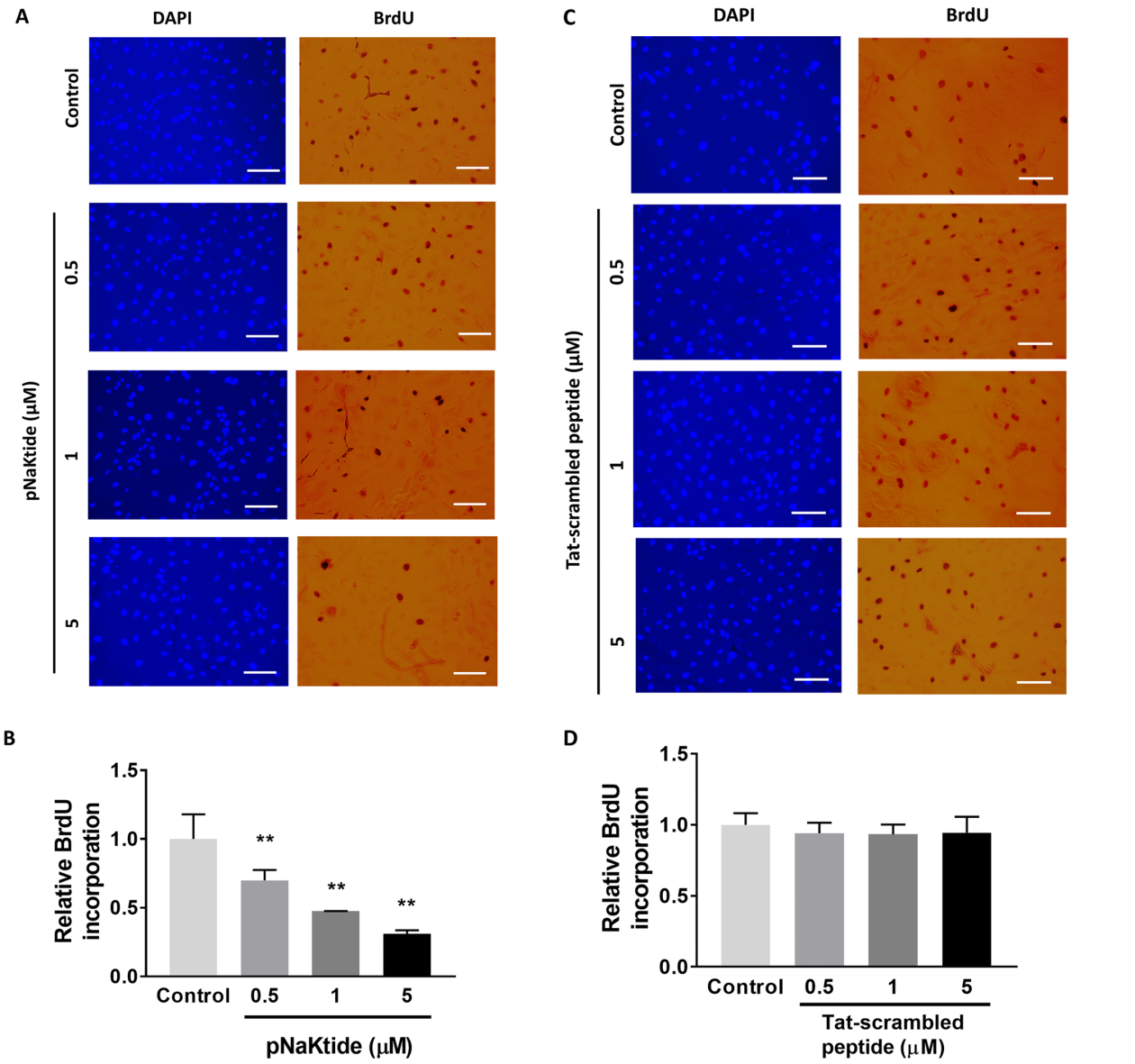

Figure 1. pNaKtide inhibits HRMEC proliferation. HRMECs were incubated with 0.5, 1, or 5 μM of pNaKtide or Tat-scrambled peptide for 24 hours, and control groups were left untreated. A BrdU assay was then used to assess cell proliferation. (**A**) Representative images of proliferating cells treated with different concentrations of pNaKtide, with DAPI-labeled nuclei (*blue*). (**B**) Quantitative assessments of BrdU-positive cells. The fraction of BrdU-positive cells in the control untreated cells was normalized to 1. (**C**) Representative images of proliferating cells treated with different concentrations of Tat-scrambled peptide. (**D**) Quantitative assessments of BrdU-positive cells. The fraction of BrdU-positive cells in the control, untreated cells was normalized to 1. Each sample was tested in triplicate, and the BrdU assay was performed three independent times per group. *Scale bar*: 50 μm. Data are presented as mean ± SEM; $n = 3$; $^{**}P < 0.01$ versus control.

polymerization. Prior to the Matrigel assays, HRMECs were cultured in EGM-2 Medium to 70% confluence in 100-mm tissue culture dishes. On the day of the assay, HRMECs were harvested and resuspended in EGM-R Medium. Subsequently, HRMECs (2.0×10^5 cells/mL) were seeded on the polymerized BD Matrigel Matrix GFR in EGM-R Medium, supplemented with the indicated concentrations of pNaKtide, and incubated for 24 hours at 37°C. Tubes were observed using a ZEISS Axio Observer microscope (Carl Zeiss Microscopy, White Plains, NY, USA) at 5× magnification. At least three independent fields per sample were captured. Tube networks were measured by a blinded investigator to determine the total tube length and total tube numbers per field using ImageJ (National Institutes of Health, Bethesda, MD, USA) with the Angiogenesis Analyzer plugin, as described previously.[39,40] The data were normalized to controls. Each sample was tested in triplicate, and the entire experiment was performed three separate times.

Animal Care

All animal studies were approved by and performed in accordance with the Marshall University Institutional Animal Care and Use Committee and the ARVO Statement for the Use of Animals in Ophthalmic and Vision Research. Pregnant C57BL/6J mice and 12-week-old male C57BL/6J mice were obtained from The Jackson Laboratory (000664; Bar Harbor, ME, USA). Mice were maintained at 24°C ± 0.5°C under a

12-hour light/dark cycle. Forty-eight neonates (offspring of the pregnant mice) were exposed to the OIR protocol detailed in the Methods section (also see Fig. 3A). Another 36 neonates were used at the age of 12 days to study pNaKtide safety and distribution after intravitreal injection, as detailed below. Twenty-four adult male mice (12 weeks old) were used to study the retinal distribution of rhodamine-labeled pNaKtide and the safety of intravitreal injection of increasing concentrations of pNaKtide, as detailed below.

Intravitreal Injections

Neonates or adult male C57Bl6/J mice were anesthetized by intraperitoneal injection of ketamine/xylazine. Intravitreal injections were performed using a 36-gauge needle and a NanoFil microsyringe (World Precision Instruments, Inc., Sarasota, FL, USA), as described previously.[41] The needle was inserted from the limbus with a 45° angle into the vitreous chamber, avoiding touching the lens. The position of the needle was monitored throughout the procedure under a dissecting microscope. After injection, mice were placed on a heating pad and monitored until fully recovered from anesthesia prior to being returned to regular housing conditions.

Toxicity Studies. A range of pNaKtide doses was defined based on efficacy and toxicity data obtained in vitro using the HRMEC model. One microliter of sterile PBS alone (left eye) or with pNaKtide (0.25, 1, or 2.5 µg, right eye) was injected in C57Bl/6J neonates at postnatal day 12 (P12; three mice per dose). This toxicity study was repeated in C57Bl/6J neonates with exposure to hyperoxia at P12 (three mice per dose). To test the toxicity of pNaKtide in adult mice, 1 µL of sterile PBS alone (left eye) or with pNaKtide (0.25, 1, 2.5, 5 or 10 µg, right eye) was injected in 12-week-old males (three mice per dose).

Efficacy in the Oxygen-Induced Retinopathy Model. One microliter of sterile PBS alone (left eye) or pNaKtide (2.5 or 25 ng, right eye) were injected in neonates at P12 exposed to an oxygen-induced protocol (see Fig. 3A).

Retinal Distribution of Rhodamine-Labeled pNaKtide

C57BL/6J mice (12-week-old males) were injected intravitreally with 1 µL of vehicle (sterile PBS, right eye) or 125 ng of rhodamine-labeled pNaKtide dissolved in sterile PBS (left eye). Three, 24, and 48 hours after injection, nine mice were euthanized by intraperitoneal injection of pentobarbital, and their eyes were enucleated. Retinas were dissected, rinsed with cold 1× PBS and flattened as described previously.[35] A similar study was done in C57BL/6J neonatal mice with exposure to hyperoxia at P12 (three mice per group). Images were obtained with a ZEISS Axio Observer microscope.

Histological Analysis

At P12, neonates received intravitreal injections of 1 µL of sterile PBS alone (vehicle, left eye) or with pNaKtide (0.25, 1, 2.5, or 5 µg, right eye; three mice per group). At P12, OIR neonates with exposure to hyperoxia received intravitreal injections of 1 µL of pNaKtide (0.25, 1, 2.5, or 5 µg, right eye; three mice per group) or sterile PBS (vehicle, left eye). Twelve-week-old male C57BL/6J mice received intravitreal injections of 1 µL of sterile PBS alone (vehicle, left eye) or with pNaKtide (0.25, 1, 2.5, or 10 µg, right eye; three mice per group). All mice were euthanized 7 days after injection, and their eyes were enucleated. The enucleated eyes used for histological analyses were fixed in Davidson's fixative and subsequently embedded in paraffin. Serial sections, 4 µm thick, were prepared from paraffin blocks. Sections were deparaffinized and hydrated using sequential immersion in xylene and graded alcohol solution. The sections were then mounted on glass slides and stained with hematoxylin and eosin (H&E). The thickness of the outer nuclear layer (ONL) and inner nuclear layer (INL) were measured in all sections by a blinded investigator using Aperio ImageScope software.

Mouse Model of Oxygen-Induced Retinopathy

Oxygen-induced retinopathy was induced in the neonatal mouse model as described previously.[42,43] At P7, neonates and nursing mothers were placed in an oxygen chamber attached to an oxygen controller (Pro-Ox 110; BioSpherix, Parish, NY, USA) and exposed to 75% ± 2% oxygen levels. After 5 days, at P12, neonates received intravitreal injections of 1 µL of pNaKtide in sterile PBS (2.5 or 25 ng) or vehicle (sterile PBS) in the right and left eyes, respectively (n = 8–13 per group), and were transferred to room air for 5 days. Neonates and nursing mothers were monitored closely (twice a day), and surrogate dams were substituted in the rare cases of death of the nursing dams. To control for possible inter-litter variability, neonates from each litter were randomized as follows: room air (raised by a surrogate mother post day 7), OIR neonates receiving PBS as a vehicle, or OIR+ pNaKtide treatment groups. For each group, the data were analyzed using neonates from at least three different litters. Pups were euthanized on P17. Mice with body weight lower than 6 g (P17) were excluded from analysis.

Retinal Vasculature Staining and Imaging

Eyes for flat mounting were enucleated and fixed in 4% paraformaldehyde for 1 hour. Retinas were isolated after fixing and stained with 500 µL lectin solution (10 µg/µL in 1-mM $CaCl_2$ in PBS; Invitrogen Alexa Fluor 594, I21413; Thermo Fisher Scientific, Waltham, MA, USA) overnight. The retinal cups were cut into quadrants and flat mounted. Immunostained flat mounted retinas were imaged using a ZEISS Axio Observer microscope. Individual images of retinal quadrants were taken at 5× magnification and merged using Photoshop (Adobe, San Jose, CA, USA). The resulting composite image of the whole retinal flat mount was used for subsequent image analysis.[42]

Quantitative Analysis of Retinal Vascular Status

The quantification of total area, central avascular region, and total vascular content was performed using differences in grayscale intensity. We determined that there were ranges of intensity that distinguished among the background avascular tissue, normal nonvascular tissue, and vascular tissue. We could not distinguish between neovascularization and normal vessels on the basis of grayscale image, so instead we used the differences in the amount of vascular tissue compared with the room air (RA) controls to indicate the quantity of neovascularization.

Investigative Ophthalmology & Visual Science

For these analyses, we used a routine in R (R Foundation for Statistical Computing, Vienna, Austria)[44] employing the EBImage package[45–48] (R code detailed is detailed in Supplementary Appendix S1), which was automated. High-resolution images of the entire retina (2048 × 2048 pixels) were read into the software, and the image was blurred by decreasing resolution to 512 × 512 pixels. Next, thresholds for background and vascular tissue were applied. Masks were then created that determined the denominator (e.g., total tissue) as well as the vascular tissue. This strategy was repeated on a central portion of the retina sized at 300 × 300 pixels, chosen to measure the central avascular component using appropriate thresholds. Image deconstruction for this process is illustrated in Supplementary Figure S6. Following the automated analysis of all images, the deconstructed masks were compared to the original images by an unbiased observer blinded to the experimental group from which the image was obtained. In some cases where the automated routine applied inaccurate masks, the thresholds were determined on the actual image, and the routine was reapplied. When such thresholds were altered, the analyses were performed with the analysis blinded to the experimental group.

Assessment of Protein Carbonylation and Western Blot Analyses in Retinal Protein Lysates

The retinal tissue was homogenized in 250 µL of ice-cold radioimmunoprecipitation assay buffer containing 1% Nonidet P-40, 0.25% sodium deoxycholate, 150-mM NaCl, 1-mM EDTA, 1-mM phenylmethylsulfonyl fluoride, 1-mM sodium orthovanadate, 1-mM NaF, 10 µg/mL aprotinin, 10 µg/mL leupeptin, and 50-mM Tris-HCl (pH 7.4). Tissue lysates were centrifuged at 16,000*g* for 15 minutes, and the supernatants were used for protein carbonylation and western blot analyses. Specifically, protein carbonylation was measured by ELISA (BioCell Protein Carbonyl Assay Kit; BioCell Corp., Auckland, New Zealand) according to the manufacturer's protocol. Determination of α1 NKA, HIF-1α, and VEGF by western blot was done following sodium dodecyl sulfate–polyacrylamide gel electrophoresis (SDS-PAGE) and transfer onto nitrocellulose using 40 µg of retinal lysate, as modified from our previously reported protocol,[38] and the following antibodies: anti-NASE (Texas Tech University, Lubbock, TX, USA), anti-HIF-1α (sc-13515; Santa Cruz Biotechnology, Dallas, TX, USA), and anti-VEGFA antibody (ab46154, Abcam, Cambridge, UK). Alpha-tubulin was used to ensure uniform sample loading in all western blots.

Quantitative RT-PCR

Retinas were collected and flash frozen in liquid nitrogen, then stored at –80°C for 1 month or less until RNA isolation. Total retinal RNA was isolated using the RNeasy Mini Kit (Qiagen, Hilden, Germany),[36] and RNA concentration was assessed using a NanoDrop 2000 (Thermo Fisher Scientific). For all samples, the A260/280 and A260/230 ratios were between 1.8 and 2.1. Single-stranded cDNA was synthesized using SuperScript III First-Strand Synthesis SuperMix (11752-050; Thermo Fisher Scientific). Briefly, 1 µg of total RNA was used to synthesize 20 µL of cDNA using SuperScript III Reverse Transcriptase. Reactions were incubated at 25°C for 10 minutes, 50°C for 30 minutes, and 85°C for 5 minutes using a Bio-Rad thermocycler (Bio-Rad Laboratories, Inc., Hercules, CA, USA), then placed on ice. The reaction mixture was treated with 1 µL RNaseH and incubated at 37°C for 20 minutes, and the cDNA was then stored at –20°C before use in quantitative PCR. All primers were synthesized by Integrated DNA Technologies (Coralville, IA, USA) (Supplementary Table S2), and primer efficiency was calculated based on the slope of a concentration curve. Real-time PCR was performed on a Roche LightCycler II using LightCycler 480 SYBR Green I Master Mix (04707516001), with 1 µL cDNA per well in a 384-well plate, and each sample was run in triplicate. After completion of the thermocycler protocol, a melt curve was generated to determine PCR product specificity; the melting temperatures (T_m) of the PCR products for each primer set are listed in Supplemental Table S2. Data analysis was performed using the $\Delta\Delta$Ct method, with *GAPDH* as a reference gene as previously described.[49] Ct values were determined using Roche 480 software, with the threshold for each plate set in the linear phase of the reaction curves. Each reaction was run in triplicate and therefore generated three Ct values. Fold change was calculated according to the following equation: Fold change $= 2^{-(\Delta Ctsample - \Delta Ctcontrol)}$, where ΔCt_{sample} = median $Ct_{gene\ of\ interest}$ – median $Ct_{reference\ gene}$, and $\Delta Ct_{control}$ refers to the average of all control ΔCt values for each plate.

Statistical Analysis

All results were plotted using Prism (GraphPad, La Jolla, CA, USA) and expressed as mean ± SEM. Data were analyzed using unpaired *t*-test or one-way ANOVA followed by Tukey's correction for multiple comparisons. $P < 0.05$ was considered significant.

Results

pNaKtide Dose-Dependently Inhibits Proliferation and Tube Formation of Human Retinal Microvascular Endothelial Cells

HRMECs were incubated with 0.5, 1, and 5 µM of pNaKtide for 24 hours, and a BrdU assay was used to assess cell proliferation.[50] As shown in Figures 1A and 1B, pNaKtide inhibited cell proliferation in a dose-dependent manner. At concentrations as low as 0.5 µM, pNaKtide significantly inhibited proliferation compared to the control (untreated) group. This anti-proliferative property was specific to the NaKtide sequence, as indicated by the lack of effect of a Tat-scrambled peptide in the same conditions (Figs. 1C, 1D). To assess the effect of pNaKtide on angiogenesis, a tube formation assay was performed as described previously.[50] The number of tubes and the average tube length per field were determined. The data were normalized to controls. As shown in Figure 2A, tube formation was significantly inhibited by pNaKtide in a dose-dependent pattern (Figs. 2B, 2D), whereas the Tat-scrambled peptide did not significantly affect HRMEC tube formation (Figs. 2C, 2E).

Retinal Distribution of Rhodamine-Labeled pNaKtide and pNaKtide-Induced Toxicity Following Intravitreal Injection

Assessment of the proposed role of α1 NKA in the pathogenesis of retinopathies in response to hypoxia/ischemia

Investigative Ophthalmology & Visual Science

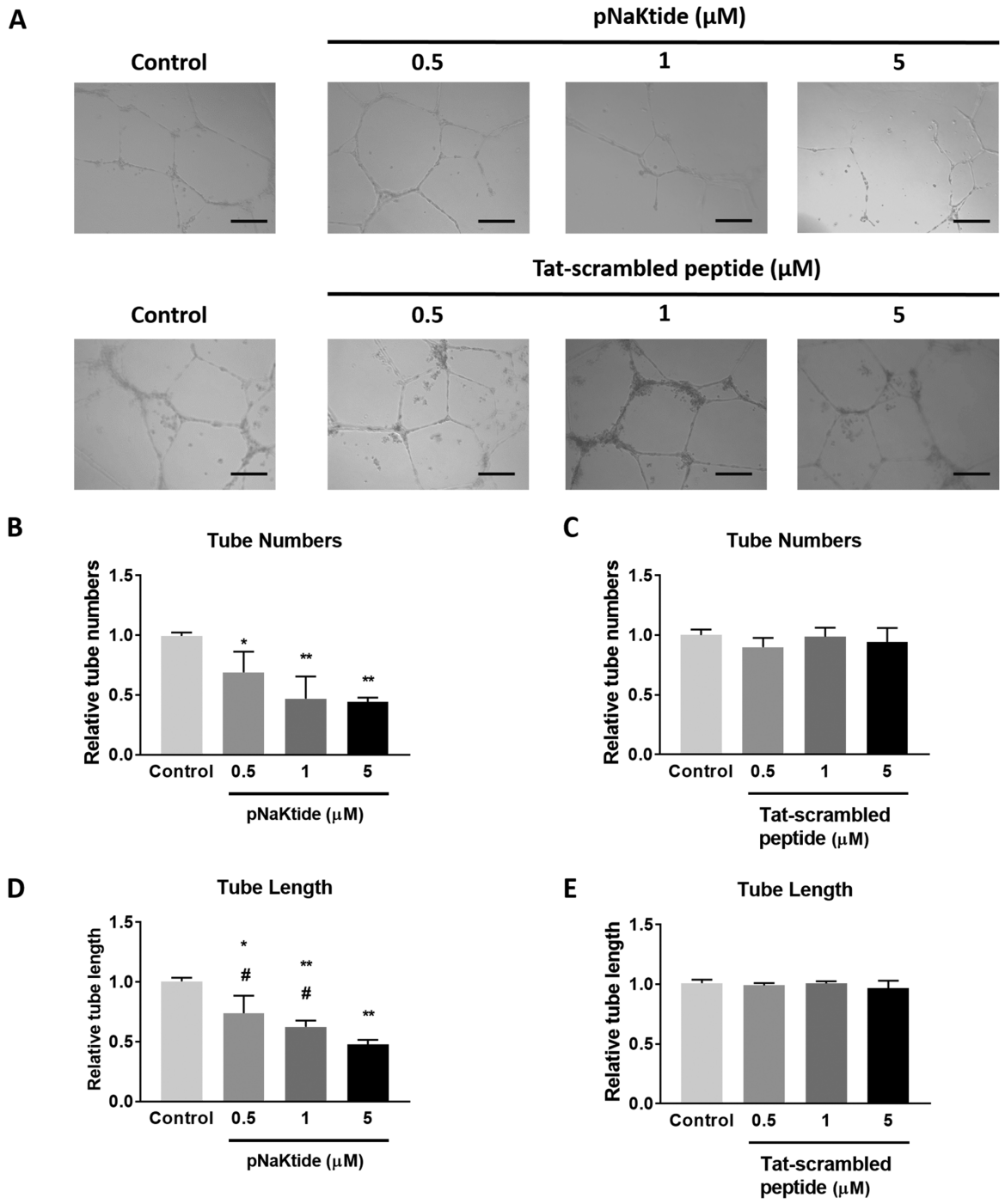

Figure 2. pNaKtide inhibits HRMECs tube formation in Matrigel. HRMECs were treated with increasing concentrations (0.5–5 μM) of the pNaKtide or Tat-scrambled peptide for 24 hours, and the control groups were left untreated. Images were captured at 5× magnification. (**A**) Representative pictures from each group. (**B**, **C**) Quantitative analysis of tube number. The number of tubes in control (untreated) was normalized to 1, and the tube numbers in treated groups were expressed relative to controls. (**D**, **E**) Quantitative analysis of tube length. The number of tubes in control (untreated) was normalized to 1, and the tube length measured in treated groups was expressed relative to controls. Each sample was tested in triplicate, and the Matrigel assay was performed three independent times. *Scale bar*: 100 μm. Data are presented as mean ± SEM; $n = 3$; $^{*}P < 0.05$, $^{**}P < 0.01$ versus control; $^{\#}P < 0.05$ versus 5-μM pNaKtide.

required in vivo pharmacological studies of pNaKtide. To this end, several control experiments were performed to determine the dosing range and route of administration. First, we tested whether pNaKtide could cross the blood–ocular barrier. Adult mice were given 25 mg/kg rhodamine-labeled (Rho) pNaKtide via intraperitoneal (IP) injection and were euthanized 3, 24, and 48 hours after injection ($n = 3$ per time point). The doses and route of administration for pNaKtide were selected because they have previously shown efficacy without toxicity when given once weekly for

up to 8 weeks in mouse models of metabolic and cardiovascular diseases.[34,35] However, although Rho fluorescence has been reported in hepatic, renal, fat, and cardiac tissues at 3 hours after injection,[35] we did not detect any indication of Rho in the retina or the brain at 3, 24, or 48 hours after injection (data not shown). Consequently, intravitreal injection was examined. In order to estimate the half-life of pNaKtide in the retina, we first isolated and imaged retinas as a function of time following intravitreal injection of 125 ng Rho–pNaKtide into the adult mouse eye. As depicted in Supplementary Figure S1A, pNaKtide showed good stability, as a significant amount of Rho fluorescence persisted 48 hours after injection. Similar studies were done in P12 OIR mouse pups with exposure to hyperoxia. pNaKtide showed a comparable stability (Supplementary Fig. S2).

The choice of the range of doses to be tested in vivo was guided by in vitro studies in HRMECs and retinal pigmented epithelial cells (ARPE-19 cells). As depicted in Supplementary Figures S1B and S1C, 50-µM pNaKtide caused a significant reduction in cell viability in HRMECs but not ARPE-19 cells. This was consistent with prior reports of nonspecific cell toxicity by Tat-tagged peptides.[51,52] Based on the reported mouse vitreous volume of about 4 to 5 µL[53] and assuming uniform distribution, we estimated that a reasonable approximation of the efficacy and toxicity of pNaKtide in the retinas of adult mice following intravitreous injection would be about 0.01 and 1 µg of pNaKtide per eye, respectively. We set an even higher dose of 10 µg/eye, at which intravitreal injection of pNaKtide did cause retinal alterations. Indeed, 1 week after injection, we observed various pathologic changes, including retinal detachment and a significant decrease in the thickness of both the INL and ONL (Supplementary Fig. S3A). Based on this observation, we carried out a descending dose–response curve study of pNaKtide at 5, 2.5, 1, and 0.25 µg/eye. H&E staining of retinal sections did not reveal any retinal lesions such as retinal tear, hemorrhage, detachment, or signs of infection in any of the pNaKtide-injected or control eyes in any of the study groups. The mean thickness of both the INL and ONL was comparable among all groups (Supplementary Figs. S3B, S3C). Accordingly, we estimated the maximum tolerated dose of pNaKtide in the mouse eye to be about 5 µg/eye. These studies were repeated in 12 days old mouse neonates (Supplementary Fig. S3D) using 2.5, 1, and 0.25 µg/eye. No significant pathologic changes were found at a dose as high as 2.5 µg/eye, and the mean thickness of both the INL and ONL was comparable among different groups (Supplementary Figs. S3E, S3F). Similar studies were done in P12 mouse pups with exposure to hyperoxia. No significant pathologic changes were found (Supplementary Fig. S4).

Intravitreal Injection of pNaKtide Promotes Physiological Revascularization and Attenuates Pathologic Neovascularization in the Mouse Model of OIR

Now turning to the potential therapeutic effects of pNaKtide on ischemic retinopathies, we implemented a mouse OIR model (Fig. 3A).[42,43] Briefly, mouse pups at P7 were exposed to 75% oxygen for 5 days and then returned to room air. Immediately upon removal from the high oxygen chamber, they received intravitreal injections with vehicle (PBS) or increasing doses of pNaKtide. Control experiments showed that this OIR model produced the expected pathologic remodeling of the retina (Supplementary Fig. S5) in our hands. Moreover, intravitreal injection of PBS actually reduced both neovascularization and central avascularization, as has been reported in the literature.[6] The effects of PBS on neovascularization appeared to be much more pronounced than those on the avascular area. Significantly, these effects were directly related to the volume of injection. Thus, all subsequent experiments were conducted with equal volumes of PBS as control, and no more than 1 µL of solution was administered.

Two doses of pNaKtide were used based on our in vitro and in vivo pharmacology studies. The high dose of 25 ng/eye was estimated to produce a vitreous concentration of about 2 µM in mouse neonates, and the low dose was set at 1/10 to give a range. Five days after the injection at P12 in OIR, retinas were harvested, flat mounted, and stained with isolectin B_4–594 for imaging and analyses of the vascularization. As shown in Figure 3, vehicle-treated retinas displayed pathologic characteristics of OIR, including a large central avascular area and pathologic neovessels in the border region between vascularized and avascular areas. Neonates treated with pNaKtide showed significant increase of revascularization of the central avascular area compared to vehicle-treated controls. This effect on revascularization, which distinguishes pNaKtide from anti-VEGF,[6] was both potent and dose dependent. Indeed, a significant effect of about 50% was observed at 2.5 ng/eye, and the highest dose (25 ng/eye) reduced the avascular area by over 80% compared to vehicle-treated eyes (Fig. 3C). Comparable to anti-VEGF treatment, pNaKtide was also a potent blocker of the development of neovascular tufts in a dose-dependent manner. The highest dose almost completely eliminated OIR-induced neovascularization (Fig. 3D).

pNaKtide Normalizes ROS Signaling in the Mouse Model of OIR

Turning to the molecular mechanism, we next investigated whether the improvements of OIR by pNaKtide were accompanied by a reduction of ROS stress in retinas. Mouse pups subjected to OIR were treated with the highest dose of pNaKtide (25 ng/eye). At P17, animals were euthanized, and retinas from different treatment groups and RA controls were processed for protein carbonylation analysis as a marker for ROS stress in vivo.[34–36] As shown in Figure 4A, a significant increase in protein carbonylation was detected in vehicle-treated control OIR eyes compared to age-matched, littermate, RA controls, and this increase was significantly reduced by pNaKtide treatment.

To substantiate these findings, we measured the expression of nuclear factor E2-related factor 2 (Nrf2)-targeted genes. Indeed, it has been reported that ROS stress activates Nrf2 pathway and consequently increases the expression of intrinsic anti-oxidant systems in OIR.[7,9] Thus, we examined whether pNaKtide administration would block this induction, as it abolished the increase in protein carbonylation. As shown in Figure 4B, at P17, OIR caused a significant induction in the transcription of Nrf2 (*Nfe2l2*), as well as a large panel of Nrf2-targeted genes, including those of heme oxygenase-1 (*Ho-1*), glutathione *S*-transferase (*Gst*), glutamate–cysteine ligase catalytic subunit (*Gclc*), NAD(P)H quinone dehydrogenase 1 (*Nqo1*), and thioredoxin reductase

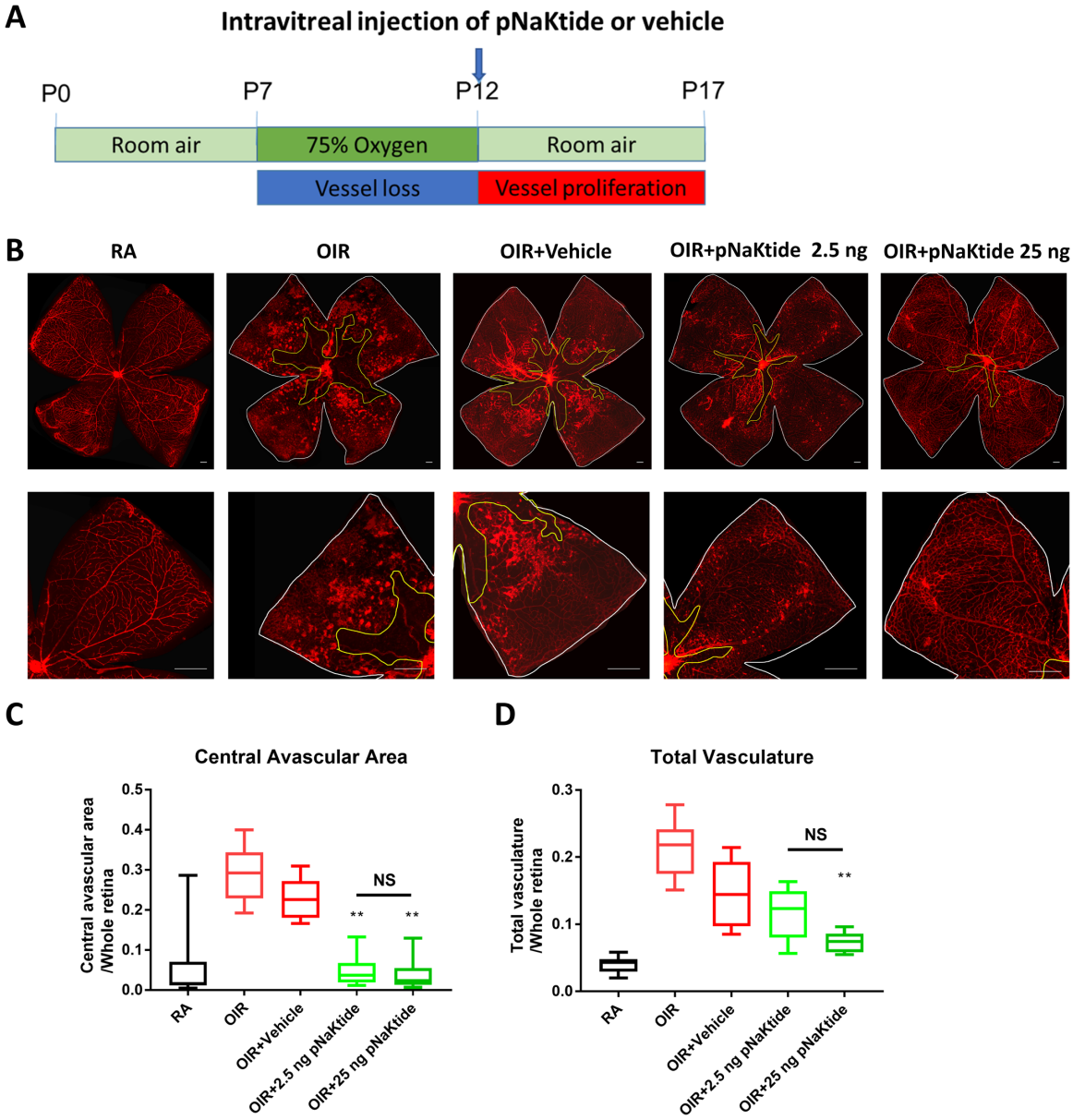

Figure 3. pNaKtide promotes revascularization and inhibits neovascularization in the mouse OIR model. (**A**) Schematic and timeline of pNaKtide treatment in the mouse model of OIR. Mice were exposed to room air (RA) or 75% oxygen (OIR) from P7 to P12. At P12, neonates received a 1-µL intravitreal injection of pNaKtide or vehicle (PBS). (**B**) (*Top*) Isolectin B4–594 stained-, flat-mounted retinas collected at P17. Central avascular and whole retinal areas are outlined with *yellow* and *white solid lines*, respectively. (*Bottom*) Pathological neovascularization and avascular areas at higher magnification. (**C**) Retinal avascular areas at P17 (ratios over respective total retinal areas). (**D**) Retinal neovascularization at P17 (ratios over their respective total retinal areas). *Scale bar*: 50 µm. Box plots present data as minimum (quartile 1 [Q1] – 1.5*IQR), median, interquartile range (IQR), and maximum (Q3 + 1.5*IQR); n = 8–13 from three to 10 litters per group. $^{**}P < 0.01$ versus OIR + PBS; NS, not significant.

1 (*Txnrd1*), as reported previously.[7–9,54,55] These increases were completely blocked by pNaKtide treatment.

Under hypoxic/ischemic conditions, the surface expression of α1 NKA in many types of cells is reduced, due to increased endocytosis.[56,57] To test whether the effectiveness of pNaKtide on ROS stress signal is related to the change in the expression of NKA in OIR, we measured the expression of the α1 subunit of NKA in whole retina by western blot (Fig. 4C). As shown in Figure 4D, no change in the expression of total retinal α1 NKA was detected in OIR.

pNaKtide Inhibited the Induction of HIF-1α and the Expression of VEGF and Other Angiogenic Factors in the Mouse Model of OIR

Under hypoxic condition, accumulated ROS upregulate HIF-1α via both transcriptional and posttranslational mechanisms in retinas.[21,22,29] In order to further validate the inhibitory effects of pNaKtide in ROS stress (Fig. 4) and to probe the mechanism of pNaKtide on OIR, we measured whether pNaKtide could inhibit hypoxia-induced

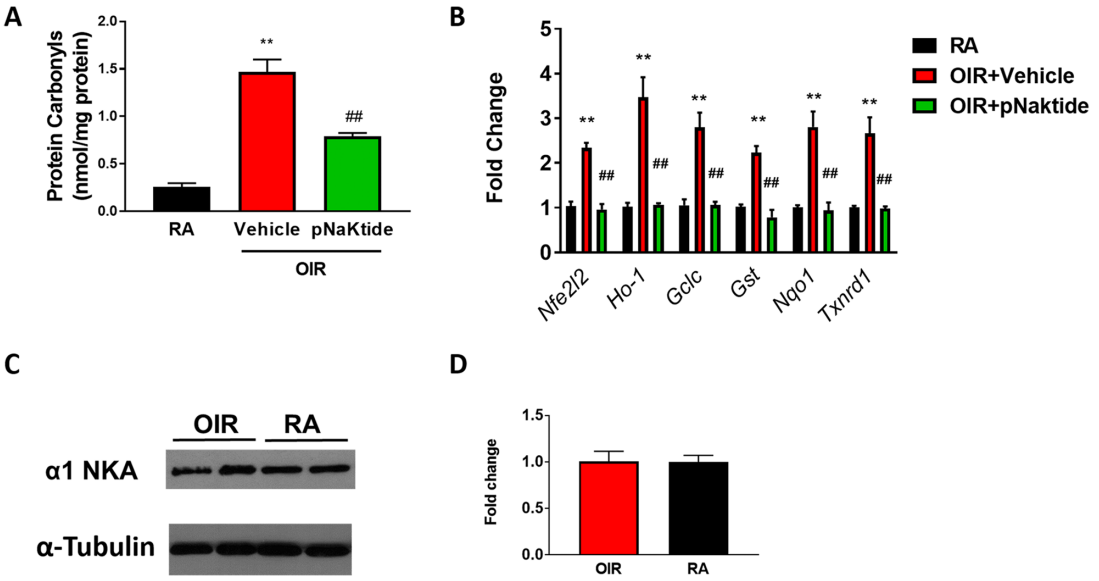

Figure 4. pNaKtide reduces ROS and Nrf2-targeted genes in the mouse model of OIR. Mice were exposed to room air or 75% oxygen from P7 to P12. At P12, mice received intravitreal injection with 1 µL of vehicle (PBS) or pNaKtide at 25 ng/eye. Retinas were dissected at P17. (**A**) Protein carbonylation content in the retinas was measured by ELISA as a ROS stress indicator. (**B**) mRNA levels of Nrf2 and Nrf2-targeted genes were assessed by RT-qPCR. (**C**) Representative western blot of α1 NKA detection in retinal tissue collected at P17. (**D**) Quantitative analysis of α1 NKA expression did not reveal a significant difference between OIR and RA groups. Data are presented as mean ± SEM; $n = 4$–9 per group; $^{**}P < 0.01$ versus RA; $^{\#\#}P < 0.01$ versus vehicle.

expression of HIF-1α. Indeed, as shown in Figure 5A, western blot analyses of whole retinas isolated from different groups of mice showed that pNaKtide at 25 ng/eye completely eliminated the increase in HIF-1α. Because HIF-1α is a key regulator of transcriptional regulation of *Vegf* expression, we next measured *Vegf* mRNA using RT-qPCR. As shown in Figure 5B, expression of *Vegf* mRNA was significantly induced in OIR retinas at P17 in comparison to those from RA control pups. Treatment with pNaKtide abolished this increase without changing the basal expression of *Vegf*. Consistently, when tissue lysates were analyzed for the expression of VEGF by western blot, we found the same pattern of changes (Fig. 5C). To assess the effects of pNaKtide on other important angiogenic factors that impact retinopathy, we also analyzed the expression of angiopoetin-2 (*Angpt2*) and erythropoietin (*Epo*). As shown in Figure 5B, the expression of *Angpt2* was completely normalized by pNaKtide treatment; however, pNaKtide significantly attenuated but did not abolish the increase in the expression of *Epo* by OIR (Fig. 5B).

pNaKtide Blocks the Increase in Inflammatory Cytokines and Collagen1a1

Increases in inflammatory cytokines play an important role in the development of OIR. To substantiate the above findings and verify the effectiveness of pNaKtide, we conducted RT-qPCR measurement of a panel of inflammatory cytokines. As shown in Figure 5D, the expression of TNF-α, IL-6, IL-1β, and C-X-C motif chemokine ligand 10 (CXCL10) mRNA was significantly induced in OIR retinas in comparison to those from RA control pups. Treatment with pNaKtide either largely attenuated or completely normalized the expression. Because pNaKtide inhibits neovascularization and inflammation, we surmised that it may also be effective in preventing tissue fibrosis. Although tissue fibrosis could not be adequately assessed in the mouse model of OIR, we did find that pNaKtide blocked an increase in *col1a1* mRNA induced by OIR (Fig. 5E).

Discussion

Normalizing excessive angiogenesis while simultaneously promoting physiological vasculature is the goal of safe and effective pharmacological intervention in ischemic diseases of the retina. This study suggests that the unique and previously unexplored regulatory mode of control of retinal ROS by the α1 NKA/Src signaling complex presents many features of a suitable prospective target. Specifically, a potential for translational application is supported by evidence that intravitreal injection of a specific blocking peptide (pNaKtide) normalized ROS signaling, inhibited neovascularization, and promoted physiological revascularization in the mouse model of ischemic retinopathy.

NKA Is a Regulator of ROS Generation, HIF-1α, and VEGF Expression in the Retina

The α1 subunit of NKA is a highly expressed plasma membrane polypeptide, represented by more than a million of units in most human cells. Only about 20% to 30% of the plasma membrane α1 NKA is engaged in ion pumping,[58] the classical function assigned to the enzymatic complex. A more recently appreciated function of α1 NKA is its enzymatic-independent receptor function through its interaction with membrane and cytosolic proteins such as Src, caveolin-1, PI3K, and EGFR.[24,38,59–62] Highly relevant in

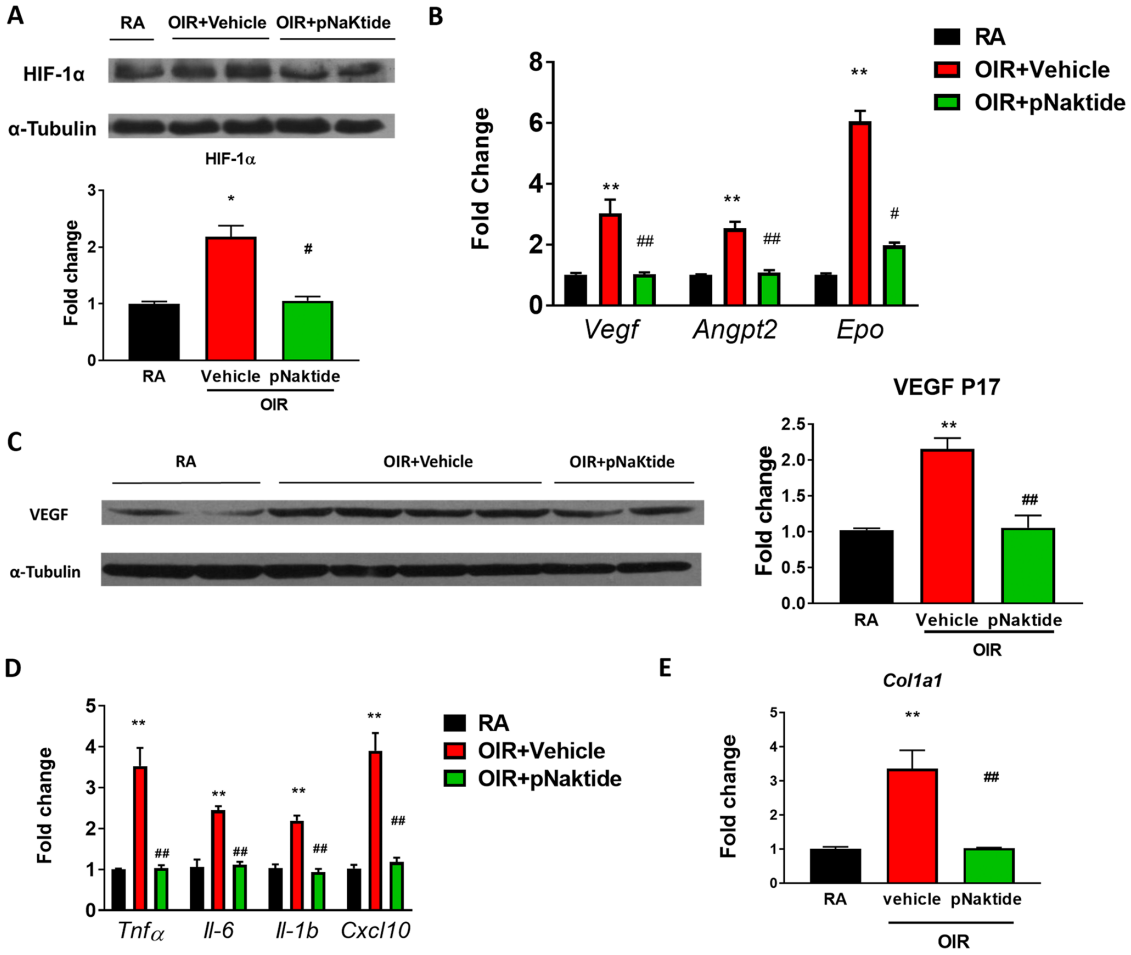

Figure 5. pNaKtide inhibits HIF-1α, VEGF and other angiogenic factors, inflammatory cytokines, and collagen 1 in the mouse model of OIR. Mouse neonates were exposed to room air or 75% oxygen from P7 to P12. At P12, mice received intravitreal injection with 1 µL of vehicle (PBS) or 25 ng pNaKtide. Retinas were dissected at P17. (**A**) Western blots and quantification of HIF-1α expression. (**B**) mRNA level of *Vegf*, *Angpt2*, and *Epo*. (**C**) VEGF expression by western blots and quantification results. (**D**) mRNA levels of inflammatory cytokines. (**E**) mRNA level of *Col1a1*. Data are presented as mean ± SEM; n = 3–6 per group; $^{*}P < 0.05$ and $^{**}P < 0.01$ versus RA; $^{\#}P < 0.05$ and $^{\#\#}P < 0.01$ versus vehicle.

the context of the present study, the α1 NKA/Src receptor complex forms a ROS amplification loop (Na/K-ATPase oxidant loop, NKAL[63]), perpetuated at least in part through H_2O_2-induced carbonylation of Pro222 and Thr224 on α1 NKA and subsequent activation of Src.[30,64] The central role of this ROS amplification mechanism in OIR was experimentally revealed by a significant reduction of retinal ROS stress when NKAL was blocked by pNaKtide (carbonyls content) (Fig. 4). Given the well-documented role of excessive ROS in the stabilization of HIF-1α and subsequent increases in the production of angiogenic factors such as VEGF in OIR,[20,65,66] a highly selective antioxidant effect of pNaKtide likely explains, at least in part, the normalization of HIF-1α and HIF-1α target genes, including VEGF in treated OIR retinas (Fig. 5). Similarly, normalization of the Nrf2 pathway and downstream endogenous antioxidant systems (e.g., *Ho-1*, *Gst*; Fig. 4) is consistent with the generation of restricted and transient ROS, rather than an excessive and inhibitory release.[54,55] Follow-up studies designed to assess the timing of molecular changes triggered by pNaKtide in the days that follow intravitreal injection may reveal time-dependent and selective regulation of ROS-dependent retinal pathways by pNaKtide.

Targeting NKAL to Develop a New Class of Therapeutics of Retinopathy of Prematurity

VEGF plays an important role in both physiological revascularization and neovascularization in animal models of ROP.[67] Although anti-VEGF therapy is effective in preventing and reversing neovascularization, it also inhibits physiological revascularization,[6,68] a major limitation to its clinical use. Recent identification of additional factors involved in pathologic vascular growth[69,70] will be beneficial to the development of new therapeutics of ROP and other ischemic eye diseases with better selectivity toward pathologic neovascularization.[10,71–73] As shown in Figures 1 to 3, pNaKtide treatment blocks retinal endothelial cell proliferation in vitro and limits neovascularization, as observed with anti-VEGF approaches.[6,74] However, unlike anti-VEGF, physiological revascularization does occur in pNaKtide-treated retinas, suggesting that the specific control of NKAL is more akin to target pathological vessel growth while preserving physiologically appropriate levels of ROS (generated in restricted amounts or in a transient fashion[75]), VEGF, and other biological mediators that are essential for physiological angiogenesis in vivo. Although the biology of vascular endothelial cells

is central to both physiological revascularization and neovascularization, it is also well known that other cell types (e.g., neurons, glia cells, or macrophages) expressing the ubiquitous α1 NKA are involved in the pathogenesis of ROP.[76–78] Thus, in addition to the role of α1 NKA signaling in vascular endothelial cells,[79] additional studies are needed to explore cell-specific roles of α1 NKA in ROP and other ischemic retinopathies. Among the most compelling non-endothelial mechanisms to be considered, the regulation of inflammatory cytokines by α1 NKA signaling in macrophages is one that deserves high priority and attention.[80] It is also noted that, although the mouse model is widely used to study OIR,[81] it differs from ROP in some of its clinical manifestations. Hence, neovascularization spontaneously regresses in the mouse model between P17 and P24,[42] whereas in human preterm infants with severe ROP the condition worsens. Second, the vaso-obliteration observed in the OIR mouse model is primarily due to constant exposure to hyperoxia, whereas the pattern of obliteration in human ROP (central vessels rather than peripheral vessels in the mouse ROI model) results from intermittent hypoxemic and hyperoxic episodes due to immature neuronal network.[82,83]

Although additional studies and models are needed to identify the key cellular players targeted by NKAL inhibition and to assess whether pNaKtide is a suitable candidate in ROP, the results of the present study suggest that "pNaKtide-like" NKA/Src inhibitors represent a new and effective strategy to explore in ischemic retinopathies. As a first-in-class candidate, pNaKtide is potent in the mouse model of OIR, with a clear and novel mechanism of action. It is important to note that pNaKtide does not inhibit the enzymatic function of NKA,[32,33] which minimizes the likelihood of effects on neuronal membrane potential or ocular volume regulation. Moreover, pNaKtide does not affect basal physiological ROS signaling or the expression of HIF-1α and VEGF. Unlike anti-VEGF-based approaches, pNaKtide has a potent and dose-dependent stimulatory effect on revascularization in addition to blocking neovascularization. Significant effects (about 50%) were observed at 2.5 ng/eye, and the highest dose (25 ng/eye) showed more than 80% reduction in avascular area compared with the vehicle-treated eye (Fig. 3C). Although still quite preliminary, the data presented in Figure 3 and Supplementary Figure S2 point to an estimated therapeutic index of pNaKtide on revascularization of 400. Hence, pNaKtide has a specific mechanism of action in the mouse OIR model, an excellent safety profile, and good pharmacokinetics in the retina, and it is well tolerated by the mouse eye.

Acknowledgments

The authors thank Carla Cook for technical support.

Supported by grants from the National Institutes of Health (R01 EY024963 and EY028100). The families of Z.X. and J.I.S. have ownership of Xipiro, a company dedicated to the development of pNaKtide as a therapy for neovascularization disorders of the eye. Patents relevant to this publication are held by the University of Toledo and Marshall University, where pNaKtide was developed and applied to ocular disorder models, respectively.

Disclosur: **J. Wang**, None; **X. Wang**, None; **Y. Gao**, None; **Z. Lin**, None; **J. Chen**, None; **J. Gigantelli**, None; **J.I. Shapiro**, Xipiro (S); **Z. Xie**, Xipiro (S); **S.V. Pierre**, None

References

1. Mintz-Hittner HA, Kennedy KA, Chuang AZ. Efficacy of intravitreal bevacizumab for stage 3+ retinopathy of prematurity. *N Engl J Med*. 2011;364(7):603–615.
2. Resnikoff S, Pascolini D, Etya'ale D, et al. Global data on visual impairment in the year 2002. *Bull World Health Organ*. 2004;82(11):844–851.
3. Campochiaro PA. Molecular pathogenesis of retinal and choroidal vascular diseases. *Prog Retin Eye Res*. 2015;49:67–81.
4. Sapieha P. Eyeing central neurons in vascular growth and reparative angiogenesis. *Blood*. 2012;120(11):2182–2194.
5. Diabetic Retinopathy Clinical Research Network. Aflibercept, bevacizumab, or ranibizumab for diabetic macular edema. *N Engl J Med*. 2015;372(13):1193–1203.
6. Tokunaga CC, Mitton KP, Dailey W, et al. Effects of anti-VEGF treatment on the recovery of the developing retina following oxygen-induced retinopathy. *Invest Ophthalmol Vis Sci*. 2014;55(3):1884–1892.
7. Uno K, Prow TW, Bhutto IA, et al. Role of Nrf2 in retinal vascular development and the vaso-obliterative phase of oxygen-induced retinopathy. *Experimental eye research*. 2010;90(4):493–500.
8. Wei Y, Gong J, Thimmulappa RK, Kosmider B, Biswal S, Duh EJ. Nrf2 acts cell-autonomously in endothelium to regulate tip cell formation and vascular branching. *Proc Natl Acad Sci USA*. 2013;110(41):E3910–E3918.
9. Wei Y, Gong J, Xu Z, et al. Nrf2 in ischemic neurons promotes retinal vascular regeneration through regulation of semaphorin 6A. *Proc Natl Acad Sci USA*. 2015;112(50):E6927–E6936.
10. Sun Y, Liu CH, SanGiovanni JP, et al. Nuclear receptor RORα regulates pathologic retinal angiogenesis by modulating SOCS3-dependent inflammation. *Proc Natl Acad Sci USA*. 2015;112(33):10401–10406.
11. Wang Y, Rattner A, Zhou Y, Williams J, Smallwood PM, Nathans J. Norrin/Frizzled4 signaling in retinal vascular development and blood brain barrier plasticity. *Cell*. 2012;151(6):1332–1344.
12. Wang H, Hartnett ME. Roles of nicotinamide adenine dinucleotide phosphate (NADPH) oxidase in angiogenesis: isoform-specific effects. *Antioxidants (Basel)*. 2017;6(2):40.
13. Joyal JS, Sun Y, Gantner ML, et al. Retinal lipid and glucose metabolism dictates angiogenesis through the lipid sensor Ffar1. *Nat Med*. 2016;22(4):439–445.
14. Wang Y, Tadjuidje E, Pandey RN, et al. The eyes absent proteins in developmental and pathological angiogenesis. *Am J Pathol*. 2016;186(3):568–578.
15. Zhu S, Liu H, Sha H, Qi L, Gao DS, Zhang W. PERK and XBP1 differentially regulate CXCL10 and CCL2 production. *Exp Eye Res*. 2017;155:1–14.
16. Liu R, Liu H, Ha Y, Tilton RG, Zhang W. Oxidative stress induces endothelial cell senescence via downregulation of Sirt6. *Biomed Res Int*. 2014;2014:902842.
17. Hoppe G, Yoon S, Gopalan B, et al. Comparative systems pharmacology of HIF stabilization in the prevention of retinopathy of prematurity. *Proc Natl Acad Sci USA*. 2016;113(18):E2516–E2525.
18. Liu Z, Yan S, Wang J, et al. Endothelial adenosine A2a receptor-mediated glycolysis is essential for pathological retinal angiogenesis. *Nat Commun*. 2017;8(1):584.
19. Wang JY, Lu Q, Tao Y, Jiang YR, Jonas JB. Intraocular expression of thymosin β4 in proliferative diabetic retinopathy. *Acta Ophthalmol*. 2011;89(5):e396–e403.
20. Wang H, Zhang SX, Hartnett ME. Signaling pathways triggered by oxidative stress that mediate features of severe retinopathy of prematurity. *JAMA Ophthalmol*. 2013;131(1):80–85.

21. Tafani M, Sansone L, Limana F, et al. The interplay of reactive oxygen species, hypoxia, inflammation, and sirtuins in cancer initiation and progression. *Oxid Med Cell Longev*. 2016;2016:3907147.
22. Wilkinson-Berka JL, Rana I, Armani R, Agrotis A. Reactive oxygen species, Nox and angiotensin II in angiogenesis: implications for retinopathy. *Clin Sci (Lond)*. 2013;124(10):597–615.
23. Skou JC. The influence of some cations on an adenosine triphosphatase from peripheral nerves. *Biochim Biophys Acta*. 1957;23(2):394–401.
24. Tian J, Cai T, Yuan Z, et al. Binding of Src to Na+/K+-ATPase forms a functional signaling complex. *Mol Biol Cell*. 2006;17(1):317–326.
25. Li Z, Xie Z. The Na/K-ATPase/Src complex and cardiotonic steroid-activated protein kinase cascades. *Pflügers Arch*. 2009;457(3):635–644.
26. Haas M, Askari A, Xie Z. Involvement of Src and epidermal growth factor receptor in the signal-transducing function of Na+/K+-ATPase. *J Biol Chem*. 2000;275(36):27832–27837.
27. Liu J, Tian J, Haas M, Shapiro JI, Askari A, Xie Z. Ouabain interaction with cardiac Na+/K+-ATPase initiates signal cascades independent of changes in intracellular Na+ and Ca2+ concentrations. *J Biol Chem*. 2000;275(36):27838–27844.
28. Xie Z, Kometiani P, Liu J, Li J, Shapiro JI, Askari A. Intracellular reactive oxygen species mediate the linkage of Na+/K+-ATPase to hypertrophy and its marker genes in cardiac myocytes. *J Biol Chem*. 1999;274(27):19323–19328.
29. Ozaki H, Yu AY, Della N, et al. Hypoxia inducible factor-1alpha is increased in ischemic retina: temporal and spatial correlation with VEGF expression. *Invest Ophthalmol Vis Sci*. 1999;40(1):182–189.
30. Yan Y, Shapiro AP, Haller S, et al. Involvement of reactive oxygen species in a feed-forward mechanism of Na/K-ATPase-mediated signaling transduction. *J Biol Chem*. 2013;288(47):34249–34258.
31. Wang Y, Ye Q, Liu C, et al. Involvement of Na/K-ATPase in hydrogen peroxide-induced activation of the Src/ERK pathway in LLC-PK1 cells. *Free Radic Biol Med*. 2014;71:415–426.
32. Li Z, Cai T, Tian J, et al. NaKtide, a Na/K-ATPase-derived peptide Src inhibitor, antagonizes ouabain-activated signal transduction in cultured cells. *J Biol Chem*. 2009;284(31):21066–21076.
33. Li Z, Zhang Z, Xie JX, et al. Na/K-ATPase mimetic pNaKtide peptide inhibits the growth of human cancer cells. *J Biol Chem*. 2011;286(37):32394–32403.
34. Sodhi K, Maxwell K, Yan Y, et al. pNaKtide inhibits Na/K-ATPase reactive oxygen species amplification and attenuates adipogenesis. *Sci Adv*. 2015;1(9):e1500781.
35. Liu J, Tian J, Chaudhry M, et al. Attenuation of Na/K-ATPase mediated oxidant amplification with pNaKtide ameliorates experimental uremic cardiomyopathy. *Sci Rep*. 2016;6:34592.
36. Sodhi K, Srikanthan K, Goguet-Rubio P, et al. pNaKtide attenuates steatohepatitis and atherosclerosis by blocking Na/K-ATPase/ROS amplification in C57Bl6 and ApoE knockout mice fed a Western diet. *Sci Rep*. 2017;7(1):193.
37. Hangaard L, Bouzinova EV, Staehr C, et al. Na-K-ATPase regulates intercellular communication in the vascular wall via cSrc kinase-dependent connexin43 phosphorylation. *Am J Physiol Cell Physiol*. 2017;312(4):C385–C397.
38. Wang X, Cai L, Xie JX, et al. A caveolin binding motif in Na/K-ATPase is required for stem cell differentiation and organogenesis in mammals and *C. elegans*. *Sci Adv*. 2020;6(22):eaaw5851.
39. Morais C, Ebrahem Q, Anand-Apte B, Parat MO. Altered angiogenesis in caveolin-1 gene-deficient mice is restored by ablation of endothelial nitric oxide synthase. *Am J Pathol*. 2012;180(4):1702–1714.
40. DeCicco-Skinner KL, Henry GH, Cataisson C, et al. Endothelial cell tube formation assay for the in vitro study of angiogenesis. *J Vis Exp*. 2014;91:e51312.
41. Venkatesh A, Ma S, Langellotto F, Gao G, Punzo C. Retinal gene delivery by rAAV and DNA electroporation. *Curr Protoc Microbiol*. 2013;Chapter 14:Unit 14D.4.
42. Connor KM, Krah NM, Dennison RJ, et al. Quantification of oxygen-induced retinopathy in the mouse: a model of vessel loss, vessel regrowth and pathological angiogenesis. *Nat Protoc*. 2009;4(11):1565–1573.
43. Smith LE, Wesolowski E, McLellan A, et al. Oxygen-induced retinopathy in the mouse. *Invest Ophthalmol Vis Sci*. 1994;35(1):101–111.
44. R Team. *R: A Language and Environment for Statistical Computing*. Vienna, Austria: R Foundation for Statistical Computing; 2019.
45. Pau G, Fuchs F, Sklyar O, Boutros M, Huber W. EBImage–an R package for image processing with applications to cellular phenotypes. *Bioinformatics*. 2010;26(7):979–981.
46. Barthelme S. imager: image processing library based on 'CImg'. Available at: https://cran.r-project.org/web/packages/imager/index.html. Accessed November 20, 2020.
47. Ooms J. magick: advanced graphics and image-processing in R. Available at: https://cran.r-project.org/web/packages/magick/index.html. Accessed November 20, 2020.
48. Wickham H. *ggplot2: Elegant Graphics for Data Analysis*. New York: Springer-Verlag; 2016.
49. Adachi H, Tominaga H, Maruyama Y, et al. Stage-specific reference genes significant for quantitative PCR during mouse retinal development. *Genes Cells*. 2015;20(8):625–635.
50. Capozzi ME, McCollum GW, Savage SR, Penn JS. Peroxisome proliferator-activated receptor-beta/delta regulates angiogenic cell behaviors and oxygen-induced retinopathy. *Invest Ophthalmol Vis Sci*. 2013;54(6):4197–4207.
51. El-Andaloussi S, Jarver P, Johansson HJ, Langel U. Cargo-dependent cytotoxicity and delivery efficacy of cell-penetrating peptides: a comparative study. *Biochem J*. 2007;407(2):285–292.
52. Saar K, Lindgren M, Hansen M, et al. Cell-penetrating peptides: a comparative membrane toxicity study. *Anal Biochem*. 2005;345(1):55–65.
53. Remtulla S, Hallett PE. A schematic eye for the mouse, and comparisons with the rat. *Vision Res*. 1985;25(1):21–31.
54. Rushmore TH, Morton MR, Pickett CB. The antioxidant responsive element. Activation by oxidative stress and identification of the DNA consensus sequence required for functional activity. *J Biol Chem*. 1991;266(18):11632–11639.
55. Nguyen T, Nioi P, Pickett CB. The Nrf2-antioxidant response element signaling pathway and its activation by oxidative stress. *J Biol Chem*. 2009;284(20):13291–13295.
56. Liu J, Kesiry R, Periyasamy SM, Malhotra D, Xie Z, Shapiro JI. Ouabain induces endocytosis of plasmalemmal Na/K-ATPase in LLC-PK1 cells by a clathrin-dependent mechanism. *Kidney Int*. 2004;66(1):227–241.
57. Belliard A, Sottejeau Y, Duan Q, Karabin JL, Pierre SV. Modulation of cardiac Na+,K+-ATPase cell surface abundance by simulated ischemia-reperfusion and ouabain preconditioning. *Am J Physiol Heart Circ Physiol*. 2013;304(1):H94–H103.
58. Liang M, Tian J, Liu L, et al. Identification of a pool of non-pumping Na/K-ATPase. *J Biol Chem*. 2007;282(14):10585–10593.
59. Liang M, Cai T, Tian J, Qu W, Xie ZJ. Functional characterization of Src-interacting Na/K-ATPase using RNA interference assay. *J Biol Chem*. 2006;281(28):19709–19719.

60. Nguyen AN, Jansson K, Sanchez G, et al. Ouabain activates the Na-K-ATPase signalosome to induce autosomal dominant polycystic kidney disease cell proliferation. *Am J Physiol Renal Physiol*. 2011;301(4):897–906.
61. Wang H, Haas M, Liang M, et al. Ouabain assembles signaling cascades through the caveolar Na+/K+-ATPase. *J Biol Chem*. 2004;279(17):17250–17259.
62. Liu J, Liang M, Liu L, Malhotra D, Xie Z, Shapiro JI. Ouabain-induced endocytosis of the plasmalemmal Na/K-ATPase in LLC-PK1 cells requires caveolin-1. *Kidney Int*. 2005;67(5):1844–1854.
63. Sodhi K, Nichols A, Mallick A, et al. The Na/K-ATPase oxidant amplification loop regulates aging. *Sci Rep*. 2018;8(1):9721.
64. Yan Y, Shapiro AP, Mopidevi BR, et al. Protein carbonylation of an amino acid residue of the Na/K-ATPase α1 subunit determines Na/K-ATPase signaling and sodium transport in renal proximal tubular cells. *J Am Heart Assoc*. 2016;5(9):e003675.
65. Al-Shabrawey M, Bartoli M, El-Remessy AB, et al. Inhibition of NAD(P)H oxidase activity blocks vascular endothelial growth factor overexpression and neovascularization during ischemic retinopathy. *Am J Pathol*. 2005;167(2):599–607.
66. Okuno Y, Nakamura-Ishizu A, Otsu K, Suda T, Kubota Y. Pathological neoangiogenesis depends on oxidative stress regulation by ATM. *Nat Med*. 2012;18(8):1208–1216.
67. Penn JS, Madan A, Caldwell RB, Bartoli M, Caldwell RW, Hartnett ME. Vascular endothelial growth factor in eye disease. *Prog Retin Eye Res*. 2008;27(4):331–371.
68. Lutty GA, McLeod DS, Bhutto I, Wiegand SJ. Effect of VEGF trap on normal retinal vascular development and oxygen-induced retinopathy in the dog. *Invest Ophthalmol Vis Sci*. 2011;52(7):4039–4047.
69. Wilkinson-Berka JL, Deliyanti D, Rana I, et al. NADPH oxidase, NOX1, mediates vascular injury in ischemic retinopathy. *Antioxid Redox Signal*. 2014;20(17):2726–2740.
70. Wei Y, Gong J, Xu Z, Duh EJ. Nrf2 promotes reparative angiogenesis through regulation of NADPH oxidase-2 in oxygen-induced retinopathy. *Free Radic Biol Med*. 2016;99:234–243.
71. Stahl A, Joyal JS, Chen J, et al. SOCS3 is an endogenous inhibitor of pathologic angiogenesis. *Blood*. 2012;120(14):2925–2929.
72. Chen J, Stahl A, Krah NM, et al. Wnt signaling mediates pathological vascular growth in proliferative retinopathy. *Circulation*. 2011;124(17):1871–1881.
73. Surace EM, Balaggan KS, Tessitore A, et al. Inhibition of ocular neovascularization by hedgehog blockade. *Mol Ther*. 2006;13(3):573–579.
74. Nakao S, Arima M, Ishikawa K, et al. Intravitreal anti-VEGF therapy blocks inflammatory cell infiltration and re-entry into the circulation in retinal angiogenesis. *Invest Ophthalmol Vis Sci*. 2012;53(7):4323–4328.
75. Kim YW, Byzova TV. Oxidative stress in angiogenesis and vascular disease. *Blood*. 2014;123(5):625–631.
76. Fulton AB, Hansen RM, Moskowitz A, Akula JD. The neurovascular retina in retinopathy of prematurity. *Prog Retin Eye Res*. 2009;28(6):452–482.
77. Downie LE, Pianta MJ, Vingrys AJ, Wilkinson-Berka JL, Fletcher EL. Neuronal and glial cell changes are determined by retinal vascularization in retinopathy of prematurity. *J Comp Neurol*. 2007;504(4):404–417.
78. Fletcher EL, Downie LE, Hatzopoulos K, et al. The significance of neuronal and glial cell changes in the rat retina during oxygen-induced retinopathy. *Doc Ophthalmol*. 2010;120(1):67–86.
79. Saunders R, Scheiner-Bobis G. Ouabain stimulates endothelin release and expression in human endothelial cells without inhibiting the sodium pump. *Eur J Biochem*. 2004;271(5):1054–1062.
80. Chen Y, Kennedy DJ, Ramakrishnan DP, et al. Oxidized LDL-bound CD36 recruits an Na+/K+-ATPase-Lyn complex in macrophages that promotes atherosclerosis. *Sci Signal*. 2015;8(393):ra91.
81. Grossniklaus HE, Kang SJ, Berglin L. Animal models of choroidal and retinal neovascularization. *Prog Retin Eye Res*. 2010;29(6):500–519.
82. Di Fiore JM, Martin RJ, Gauda EB. Apnea of prematurity–perfect storm. *Respir Physiol Neurobiol*. 2013;189(2):213–222.
83. Martin RJ, Di Fiore JM, Macfarlane PM, Wilson CG. Physiologic basis for intermittent hypoxic episodes in preterm infants. *Adv Exp Med Biol*. 2012;758:351–358.

Investigative Ophthalmology & Visual Science